High Performance Catalytic Tubular Membrane Reactors Owing to Forced Convective Flow Operation

Frerich J. Keil[*], Uta Flügge

Hamburg University of Technology, Chemical Reaction Engineering,
Eissendorfer Str. 38, D-21073 Hamburg, Germany

Various tubular membranes were operated as catalyst supports whereby a radial convective flux of reactants through the pores was generated. A remarkable feature of convective flux through catalytic membranes is the very low catalyst loading necessary for a high conversion. Additionally, this mode of operation allows a control of contact time of the reactants with the catalyst which can improve the reaction selectivity. The influence of catalyst preparation methods was investigated. Very high conversions of H_2O_2 decomposition could be obtained for production plant waste water over a long period of time. A reactor model was used for simulations of the experiments.

Keywords: Membrane reactor, forced convective flow, short-contact-time reactor, hydrogen peroxide decomposition

Introduction

Membrane reactors combine reaction and separation in a single unit operation. In most cases the membrane removes one or more of the reaction or product species. The yield of reactions, which are limited by thermodynamic equilibrium, can be increased beyond their equilibrium values by removing the products. The membrane can act as a catalyst either being catalytic by itself or by being impregnated with a catalyst. In some cases packed or fluidized beds of catalysts exist inside or outside the membranes. Membrane reactors are in use in biotechnology at a low temperature level. The first high-temperature catalytic membrane reactors in operation employed metallic palladium (or Pd alloy) membranes. Palladium membranes were the first to be used in catalytic membrane reactor applications because of their specific H_2 permselectivity. Micro-porous ceramic membranes can at best separate the various gases according to the Knudsen diffusion law. Their permeabilities are inversely proportional to the square root of molecular weights. Zeolite or carbon membranes and some membranes manufactured by specialized techniques (e.g. CVD procedures) have molecular sieving properties. Reviews on membrane reactors were presented by Hsieh [1,2], Zaspalis and Burggraaf [3], Saracco and Specchia [4], Zaman and Chakma [5], Dalmon [6] and Coronas and Santamaria [7]. Models are reviewed by Tsotsis et al. [8]. A comprehensive review of catalytic reactors was presented by Marcano and Tsotsis [9].

Contrary to the previously mentioned mode of operation, in the present paper various tubular porous membranes will be employed as a catalyst support whereby radial forced convective flux of reactants through the pores is generated. In fact, it is a radial flow reactor with narrow pores. One can imagine this reactor as a radial flow reactor filled with catalytic pellets whereby the pellets were crushed such that the interstitial volume is reduced to narrow pores. The pore size distribution has to be optimized according to suitable criteria. The molecular sieve effect of the membrane is not used. Owing to the forced convective flux, which is far higher than a diffusive flux, a very good contact between reactants and catalyst particles can be achieved which causes a high conversion even for very low catalyst loadings. This reactor concept was introduced in a thesis by Flügge [10]. The concept of forced-flow membrane reactors with catalyst located inside the membrane pores was reported only in very few papers [11-14]. By varying the inlet pressure one can control the convective flux, and as a consequence the contact time of the reactants with the catalyst, which in turn allows one to control the reaction selectivity to a certain extent. This reactor can also be considered as a short-contact-time reactor.

As an example the H_2O_2 decomposition at palladium catalyst on different membranes was chosen. The H_2O_2 content of waste water from H_2O_2 plants is quite high

---

*Contact information: E-mail: keil@tu-harburg.de

and has to be degraded. Furthermore, this reaction should serve as an example for the testing of membrane catalysts under convective flow which, later on, should be used for the synthesis of high-grade chemicals. Of course, H_2O_2 could be decomposed by suitable enzymes too.

The objectives of the present paper are:

- Various tubular membranes under radial flux were tested for the H_2O_2 decomposition reaction.
- The influence of the catalyst preparation methods was investigated (impregnation immobilization of the catalyst, reduction).
- The kinetics of the H_2O_2 decomposition was determined.

Table 1 Properties of the membranes employed

Type of membrane	Pore radii [μm]	Inner diameter [mm]	Outer diameter [mm]	Pore volume [ml/g]	Isoelectric points (pH)
1) α-Alumina	3.0	6	10	0.1038	7.4
2) α-Alumina	0.2	6	10	0.112	7.9
3) Carbon	0.14	6	10	0.215	5.75
4) Carbon fiber	min. 0.1	6	9	0.169	5.5
5) Polyethylene	1.0	5	9	0.353	-
6) Polypropylene	0.2	5.5	9	2.914	-

- Extensive investigations of different membranes in a pilot plant over a longer period of time should reveal the suitability of catalytic membranes under radial convective flux conditions.
- A two-dimensional model of the catalytic membrane was developed which represents the experimental results to a high degree of accuracy.
- The membranes were tested under real conditions by using production plant waste water.

Experimental

Membranes and Catalyst

Five different membrane materials were employed: α-alumina (from company PoroCer), carbon (CarboSep M14 from TechSep (Rhone-Poulenc)), carbon fiber (CFCC from Deutsche Carbone (Le Carbone Loraine)), polyethylene and polypropylene (both from Microdyn). The pore radii distributions, zero points of charge as a function of the pH-values, and the pore volumes were determined. Mercury porosimetry was employed for the determination of the pore radii. The method suggested by Brunelle [15] and Jiratova [16] was used, modified according to a paper by Ludwig and Hönicke [17] for the determination of the isolectric points. The pore volumes were found by soaking the materials with ethanol. The data obtained are presented in Table 1.

Tubular membranes were employed. The α-Alumina membranes were temperature resistant up to 1000°C and pressure resistant up to 40 bar. The 0.2 μm membrane was fixed on a support which had a maximum of the pore radii distribution at 3 μm. The carbon membrane (CarboSep M14 from the company TechSep (Rhone Poulenc)) consisted of a carbon support and a ZrO_2-TiO_2 separation layer at the inner side of the tube. The membrane was temperature resistant up to 350°C and pressure resistant up to 15 bar. The carbon fiber membrane was a asymmetric carbon-carbon fiber tube with a thin separation layer of carbon. The maximum operation temperature was 165°C and the maximum pressure 40 bar. The spectrum of pore radii was rather broad with a minimum at 0.1 μm. The maximum operation temperature of the polyethylene and polypropylene membranes was 60°C, and the maximum operating pressures were 1.5 and 3.0 bar, respectively.

Palladium was employed as a catalyst for decomposition of hydrogen peroxide. The active component should be distributed evenly over the membrane cross section. For this purpose the membranes were impregnated over 1 hour with a solution of H_2PdCl_4 (0.5 wt-% Pd). The membrane was put into such an amount of H_2PdCl_4 solution that the liquid filled the pore volume exactly. The membrane was dried for about 12 hours at room temperature. Drying at high temperatures leads to a redistribution of the palladium to the outer surfaces of the membrane. A chemical immobilization of the palladium was done after the impregnation with H_2PdCl_4 by adding NaOH (pH = 13.6) over 45 to 60 min. The following reaction occurs:

$$PdCl_4^{2-} + 4OH^- \rightarrow Pd(OH)_4^{2-} + 4Cl^- \qquad (1)$$

Owing to this treatment the palladium is immobilized. Alternatively, $NaCO_3$ (17 wt-%, pH = 11.7) was used or the dried pellets were additionally treated at 600°C. A liquid phase reduction was done at room temperature by means of $NaBH_4$:

$$NaBH_4 + 2H_2O \rightarrow NaBO_2 + 4H_2 \qquad (2)$$
$$2Pd(OH_4)^{2-} + 4H_2 \rightarrow 2Pd + 8H_2O \qquad (3)$$

$$2Pd(OH)_4^{2-} + NaBH_4 \rightarrow NaBO_2 + 2Pd + 6H_2O \qquad (4)$$
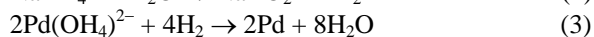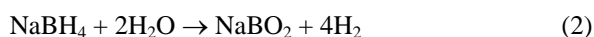
Some palladium nuclei should be present for the reduction at room temperature. The reduction solution was set to a pH-value of 12 with NaOH in order to precipitate the palladium. This measure prevents a migration of the palladium to the outer surface of the

membrane. Alternatively, the reduction was done with hydrogen diluted with nitrogen over 3 hrs at 350°C:

$$Pd(OH)_4^{2-} + 2H_2 \rightarrow Pd + 4H_2O \qquad (5)$$
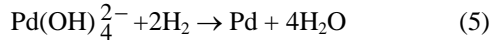
The preparation methods described above led to an evenly distributed palladium inside the membranes as was found by experimental checking. For the carbon membranes x-ray fluorescence was used for these investigations.

Kinetics of H₂O₂ decomposition

McKee [18] investigated the disproportionation of diluted aquous H₂O₂ solutions with the aid of metal

$y_{DIFF} = -6439{,}4x + 18{,}643$

$y_{INT} = -6019{,}4x + 16{,}807$
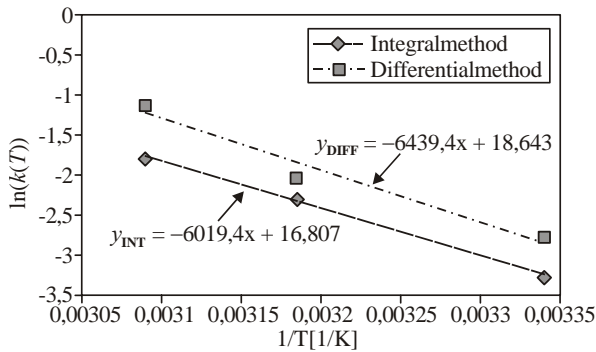
Fig. 1 Arrhenius-plot for Al₂O₃

powder of the VIII group of elements. It was found that the activity of palladium was higher than of gold. Furthermore, a strong dependence of the rate of reaction of the pH-value was detected (with a maximum at pH = 10 – 11). The kinetics was of first order and followed a postulated mechanism like this:

$$
\begin{aligned}
H_2O_2 &\rightarrow HO_2^\bullet + H^\bullet \\
H_2O_2 &\rightarrow HO^\bullet + OH^\bullet \\
HO^\bullet + H_2O_2 &\rightarrow HO_2^\bullet + H_2O \\
HO_2^\bullet + H_2O_2 &\rightarrow HO^\bullet + O_2 + H_2O \\
HO_2^\bullet + OH^\bullet &\rightarrow H_2O + O_2 \\
H^\bullet + OH^\bullet &\rightarrow H_2O \\
\hline
2H_2O_2 &\rightarrow 2H_2O + O_2 \qquad (6)
\end{aligned}
$$
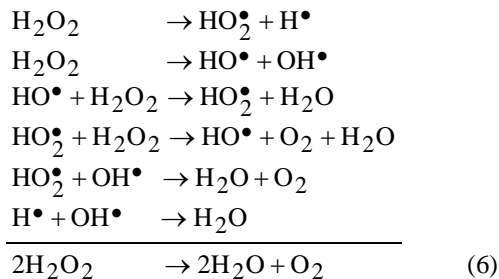
Gossner et al. [19] investigated the kinetics of H₂O₂ decomposition with a silver catalyst for an H₂O₂ concentration of less than 5 mol/l. The authors observed that the reaction was first order for a H₂O₂ concentration below 0.3 mol/l and of second order for a concentration in the range of 0.3 – 1.2 mol/l. Gossner and Bischof [20,21] published also results on the dependence of the pH value of H₂O₂ at silver and gold catalysts. They found that the reaction rate for a silver catalyst was independent of the pH value for pH < 8 and increased with the pH value above pH = 8. At a gold catalyst the reaction rate increased with increasing pH value over the entire range of the pH scale. The reaction order for a gold catalyst was two over the whole range of H₂O₂ concentrations. Eley and MacMahon [22] investigated the decomposition of highly concentrated H₂O₂

solutions at wires of palladium, gold and their alloys. A significant higher activity of gold compared to palladium was detected. The authors found first order reactions. Kreja [23] investigated the decomposition of H₂O₂ at platinum catalysts over a wide rage of H₂O₂ concentration (0.005 – 0.2 mol H₂O₂/cm³) and different specific catalyst surfaces. Again a first order reaction was detected at lower and a second order reaction at higher H₂O₂ concentrations. The transition of the reaction order depends on the specific catalyst surface. Schekhobalova [24,25] measured the kinetics of H₂O₂ decomposition at palladium and palladium/platinum alloys on alumina and silica supports. The alloys were more active than the pure metals. The reaction order was found to be about 0.7. The supports had no influence on the reaction rate.

In order to determine the reaction kinetic expressions for each experiment two liters of a 5 wt-% H₂O₂ solution were filled into a continuously stirred retort and heated to a preset temperature. The pH-value was set to 7. Before the experiment started the exact initial H₂O₂ concentration had been measured by titration with potassium permanganate. An exactly determined amount of catalyst powder (Pd on membrane support) of about 2 g was filled into the retort. After certain periods of time samples of 5 ml of the reaction mixture were taken, and immediately separated from the catalyst powder by filtering in order to prevent the solution from further reaction. The present amount of H₂O₂ was again determined by KMnO₄ titration. These measurements were repeated at different temperatures in the range from 20 to 50°C. An Arrhenius plot for an Al₂O₃ membrane is presented in Fig. 1. The experimental data were evaluated by means of the integral and differential method. Both approaches gave nearly the same results. In Table 2 some results are presented. As can be observed the reaction order with respect to the H₂O₂ concentration is equal to one for the present initial concentration. The activation energies are in the order of magnitude as found by Schekhobalova [25] (about 50 (kJ/mol)). The present authors found a transition from kinetics of first order to second order at a H₂O₂ concentration of about 65 g H₂O₂/l.

H₂O₂ decomposition measurements

For the H₂O₂ decomposition measurements an experimental set-up as given in Fig. 2 was employed. The liquid is pumped from a storage tank via a filter through the membrane. Two different pumps were used, a centrifugal pump (company Hartmann) with 2800 revolutions/min with a volume flux of 13 l/min and a membrane pump (Prominent G5) with a maximum volume flux of 9.54 l/min at a maximum counter pressure of 13 bar. The set-up can be either operated at a constant pressure or at a constant volume flux. The membranes (length 246 mm) were fixed into a tubular module by means of two o-ring seals (see Fig. 1b). The seals separate the permeate volume from the retentate and feed. At both ends of the membrane module Swagelok fittings were screwed on. For the experiments the membrane pump was used. The filter had a pore

diameter of 0.45 µm. Valve V1 was closed such that the flux passed radially through the membrane. The fluxes and the H_2O_2 content were measured every 15 minutes. The loading of the membranes with palladium had

nearly no influence on the fluxes compared to the original membranes. The results of the measurements will be discussed in a subsequent section.

Table 2 Kinetic data

Type of membrane	Pore radii [µm]	Activation energy [kJ/mol]	Reaction rate [g/(l · min)]
1) α-Alumina[1]	3.0	68.08	$6.12 \cdot 10^{10} \exp(-68.08/(8.314 \cdot T)) \cdot C_{H_2O_2}$
2) α-Alumina[2]	0.2	50.05	$1.99 \cdot 10^{7} \exp(-50.05/(8.314 \cdot T)) \cdot C_{H_2O_2}$
3) Carbon[3]	0.14	50.05	$1.99 \cdot 10^{7} \exp(-50.05/(8.314 \cdot T)) \cdot C_{H_2O_2}$
4) Carbon[4]	0.14	51.61	$1.34 \cdot 10^{6} \exp(-51.67/(8.314 \cdot T)) \cdot C_{H_2O_2}$

[1] 0.3 wt-% Pd load   [3] 0.3 wt-% Pd load
[2] 0.3 wt-% Pd load   [4] 0.06 wt-% Pd load
All the samples were treated with NaOH and reduced with $NaBH_4$
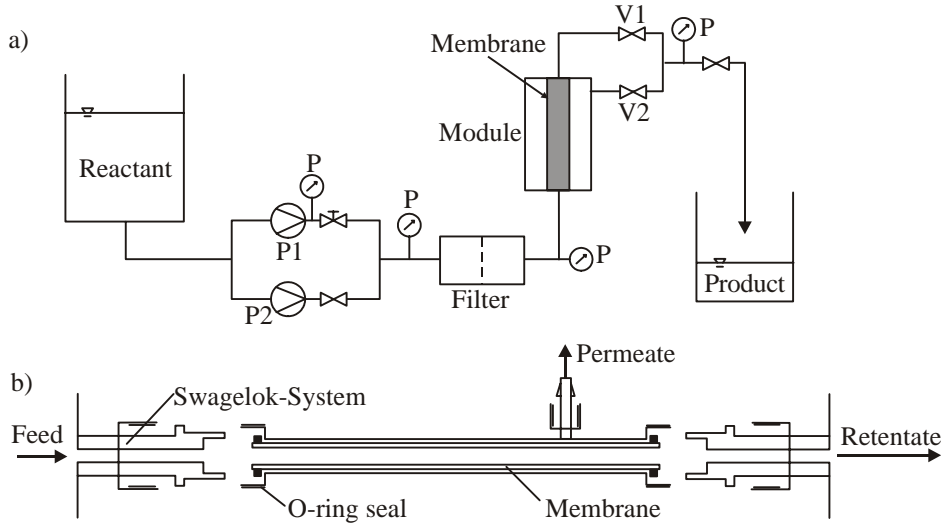
Fig. 2a Flowsheet of the test bench
2b Tubular module of the membrane reactor

Modeling

The model

The membrane reactor consists of three regions: inside the tubular membrane, the membrane, and the annulus between the membrane and the shell (see Fig. 3). For the membrane a two-dimensional model was introduced and for the other two regions a one-dimensional dispersion model was employed. These two regions are radially perfectly mixed. For the membrane a two-dimensional dispersion model was introduced (see Fig. 4). The fluid can be assumed as being incompressible such that there are no convective fluxes in axial direction inside the membrane. Now we derive a general mass balance for the inner and shell region (see Fig. 5). For a certain component we have the material balance (see notation section):

$$\frac{\partial n}{\partial t} = \dot{n}_{in} - \dot{n}_{out} + \dot{S}_{in} + \sum_{j=1}^{n_R} v_j R \cdot \varepsilon \cdot dV \qquad (7)$$

For the axial terms a Taylor expansion, truncated after the first term, gives:

$$\dot{n}_{out} = \dot{n}(x + dx) = \dot{n}(x) + \frac{\partial \dot{n}_x}{\partial x} dx \qquad (8)$$

The sum of the in- and outgoing fluxes therefore is:

$$\dot{n}_{in} - \dot{n}_{out} = -\frac{\partial \dot{n}}{\partial x} dx \qquad (9)$$

In axial direction one finds convection and dispersion:

$$\dot{n}(x) = u(x) A_R c(x) - D A_R \frac{\partial c}{\partial x} \qquad (10)$$

The derivative with respect to the length coordinate x gives:

$$\frac{\partial \dot{n}(x)}{\partial x} = A_R \left[u(x) \frac{\partial c(x)}{\partial x} + c(x) \frac{\partial u(x)}{\partial x} - D \frac{\partial^2 c}{\partial x^2} \right] \qquad (11)$$

Radial mass transfer occurs owing to a mass transfer through the boundary layer and radial convection:

$$\dot{S} = \sum_{l=1}^{n_p} A_l \beta_l (c_l - c) - c \sum_{m_{out}=1}^{n_{p,out}} |u_{r,out}| A_{m_{out}} + \sum_{m_{in}=1}^{n_{p,in}} c_{m,in} |u_{r,m_{in}}| A_{m_{in}} \quad (12)$$
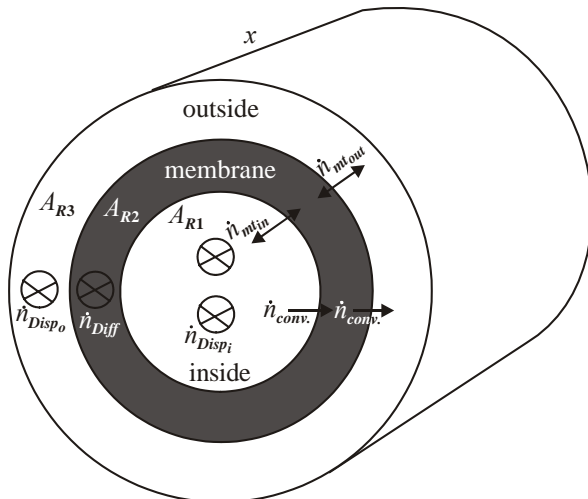
Fig. 3 Fluxes inside the reactor
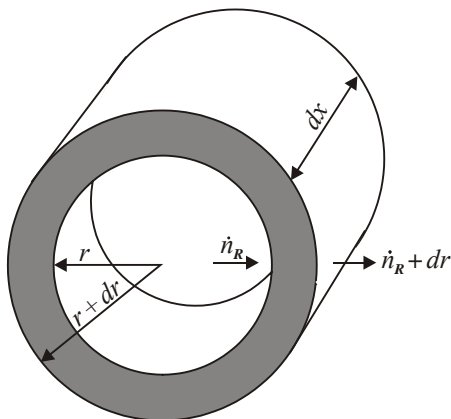
Fig. 4 Two-dimensional dispersion model of the membrane

The material balance around the element in Fig. 5 then leads to:

$$\varepsilon dV \frac{\partial c}{\partial t} = A_R \left[u(x) \frac{\partial c(x)}{\partial x} + c \frac{\partial u(x)}{\partial x} - D \frac{\partial^2 c(x)}{\partial x^2} \right] dx + \sum_{l=1}^{n_p} A_l \beta_l (c_l - c) - c \sum_{m_{out}=1}^{n_{p,out}} |u_{r,m_{out}}| A_{m_{out}} + \sum_{m_{in}=1}^{n_{p,in}} c_{m_{in}} |u_{r,m_{in}}| A_{m_{in}} + \sum_{j=1}^{n_R} v_j R \varepsilon dV \quad (13)$$

Division by $\varepsilon \cdot dV = \varepsilon A_R dx$ gives the general expression for the material balance:

$$\frac{\partial c}{\partial t} = \frac{1}{\varepsilon} \left[u(x) \frac{\partial c(x)}{\partial x} + c(x) \frac{\partial u(x)}{\partial x} - D \frac{\partial^2 c(x)}{\partial x^2} \right] + \frac{1}{\varepsilon A_R} \left[\sum_{l=1}^{n_p} a_l \beta_l (c_l - c) - c \cdot \sum_{m_{out}=1}^{n_{p,out}} |u_{r,m_{out}}| a_{m_{out}} + \sum_{m_{in}=1}^{n_{p,in}} c_{m_{in}} |u_{r,m_{in}}| a_{m_{in}} \right] + \sum_{j=1}^{n_R} v_j R$$
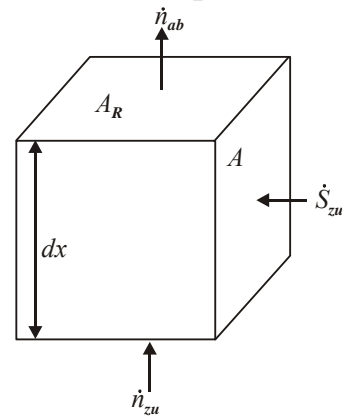
Fig. 5 Material balance around an element

This general expression can be applied to the inner region and the annulus, which results in:

$$\frac{\partial c_{inner}}{\partial t} = \left[u_{inner} \frac{\partial c_{inner}}{\partial x} + c_{inner} \frac{\partial u_{inner}}{\partial x} - D_{inner} \frac{\partial^2 c_{inner}}{\partial x^2} \right] + \frac{1}{A_{R_{inner}}} \left[a_{inner} \cdot \beta_{inner} (c_{membr} - c_{inner)-} - c_{inner} |u_{r,inner}| a_{inner} \right] \quad (15)$$

$$\frac{\partial c_{outer}}{\partial t} = \left[u_{outer} \frac{\partial c_{outer}}{\partial x} + c_{outer} \frac{\partial u_{outer}}{\partial x} - D_{outer} \frac{\partial^2 c_{outer}}{\partial x^2} \right] + \frac{1}{A_{R_{outer}}} \left[a_{outer} \cdot \beta_{outer} (c_{membr} - c_{outer)+} + c_{membr} \cdot |u_{r,outer}| \cdot a_{outer} \right] \quad (16)$$

For the membrane itself one has to introduce a two-dimensional model.

A material balance of a component is calculated over an arbitrary volume element dV (see Fig. 4).

$$\frac{\partial n}{\partial t} = \dot{n}_{in,rad,conv} - \dot{n}_{out,rad,conv} + \dot{n}_{in,ax,diff} - \dot{n}_{out,ax,diff} + \dot{n}_{in,rad,diff} - \dot{n}_{out,rad,diff} + v_i r \cdot \varepsilon dV \quad (17)$$

A Taylor series expansion of the axial material flux, truncated after the first term, gives the following result:

$$\dot{n}_{ax}(x + dx) = \dot{n}_{ax}(x) + \frac{\partial \dot{n}_{ax}}{\partial z} dx \quad (18)$$

The reasonable assumption of no pressure gradients in axial direction results in a diffusive transport in axial direction only:

$$\dot{n}_{ax,diff} = -DA_R \frac{\partial c}{\partial x} \qquad (19)$$

Thus the following result is obtained:

$$\frac{\partial \dot{n}_{ax}}{\partial x} = -DA_R \frac{\partial^2 c}{\partial x^2} = -D \frac{\partial^2 c}{\partial x^2} 2\pi r dr \qquad (20)$$

For the diffusive transport in radial direction one obtaines an analogous expression:

$$\dot{n}_{rad,diff}(r+dr) = \dot{n}_{rad,diff}(r) + \frac{\partial \dot{n}_{rad,diff}}{\partial r} \cdot dr \qquad (21)$$

The radial area depends on the position. Therefore, the following expression for the radial diffusive flux is obtained:

$$r_{rad,diff} = -DA(r) \frac{\partial c}{\partial r} = -Dr 2\pi \, dx \frac{\partial c}{\partial r} \qquad (22)$$

Partial derivation with respect to the radius results in:

$$\frac{\partial \dot{n}_{rad,diff}(r)}{\partial r} = -D2\pi dx \left(r \cdot \frac{\partial^2 c}{\partial r^2} + \frac{\partial c}{\partial r} \right) \qquad (23)$$

There is also a radial convective flux. Therefore, the following relations are obtained:

$$\dot{n}_{rad,conv} = u_{rad,}(r) \cdot c(r) \cdot A(r) =$$
$$= u_{rad}(r=r_i) \cdot \frac{A(r=r_i)}{A(r)} c(r) A(r) = \qquad (24)$$
$$= u_{rad}(r=r_i) \cdot A(r=r_i) \cdot c(r)$$

Again we obtain for the Taylor expansion:

$$\dot{n}_{rad,conv}(r+dr) = \dot{n}_{rad,conv}(x) + \frac{\partial \dot{n}_{rad,conv}}{\partial r} \cdot dr \qquad (25)$$

Partial derivation gives:

$$\frac{\partial \dot{n}_{rad,conv}}{\partial r} = u_{rad,conv}(r=r_i) \cdot A(r=r_i) \frac{\partial c}{\partial r} \qquad (26)$$

Therefore, the material balance gets the form

$$\varepsilon \cdot dV \cdot \frac{\partial c}{\partial t} = -u_{rad}(r=r_i) 2r_i \pi \frac{\partial c}{\partial r} dxdr +$$
$$+ D \frac{\partial^2 c}{\partial x^2} 2\pi r dxdr + \qquad (27)$$
$$+ D2\pi \left(r \frac{\partial^2 c}{\partial x^2} dxdr + \frac{\partial c}{\partial r} \right) + R v \varepsilon dV$$

With

$$dV = 2\pi r dr dx \qquad (28)$$

and recasting one obtains:

$$\frac{\partial c}{\partial t} = \left(-\frac{u_{rad}(r=r_i) \cdot r_i}{\varepsilon \, r} \right) + \frac{D}{\varepsilon} \frac{\partial^2 c}{\partial r^2} + \frac{D}{\varepsilon} \frac{\partial^2 c}{\partial x^2} + vR \qquad (29)$$

For the stationary case eq. (29) is an elliptical partial differential equation. In case the axial terms are dropped the equation turns to a parabolic PDE. Initially, a constant value for the concentration inside the inner ring of the membrane tube is assumed. The value is equal to the inlet concentration. Inside the membrane and outside the tube (permeate side) initially the concentration is set to zero. This situation is the case during start-up. The tube inlet $(x = 0)$ at the inner ring of the tube the concentration equals the inlet concentration all the time $c_{in}(x=0) = c_o$. Furthermore, it is assumed that there is no concentration gradient at the inner and outer side of the membrane:

$$\left. \frac{\partial c_{membr}}{\partial x} \right|_{x=0} = \left. \frac{\partial c_{membr}}{\partial x} \right|_{x=L} = \left. \frac{\partial c_{out}}{\partial x} \right|_{x=0} =$$
$$= \left. \frac{\partial c_{out}}{\partial x} \right|_{x=L} = 0 \qquad (30)$$

That means there is no diffusive and dispersive flux into the membrane. Additionally, the concentration gradient at the inlet is set to zero. This boundary condition is quite well fulfilled.

The model equations were solved by using the NAG-Library [26] routines D02NVF, D02NUF, D01NDF, and D02NXF. The integrator D01NDF is a general purpose routine for integrating the initial value problem for a stiff system of differential equations. It is designed specifically for the case where the Jacobian is a sparse matrix. The program calls the sparse matrix linear algebra setup tourine D02NUF, and the Backward Differentiation Formula (BDF) integrator routine D02NVF. D02NXF is a sparse linear algebra diagnostic routine.

Model parameters

Some model parameters have to be calculated. The diffusion coefficients of the pure components in water are calculated according to Wilke and Chang [27]:

$$D_{AB}^o = 7.4 \cdot 10^{-8} \cdot \frac{(\varphi M_B)^{0.5} T}{\eta_B V_A^{0.5}} \left[\frac{cm^2}{s} \right] \qquad (31)$$

For the association factor φ a value for water of 2.6 was taken. The molar volume V_A at the normal boiling point was calculated by means of a formula suggested by Gunn and Yamada [28]:

$$\frac{\tilde{v}}{\tilde{v}_{sc}} = V_r^o (1 - \omega \Gamma) \qquad (32)$$

whereby

$$\tilde{v}_{sc} = \frac{RT}{p_c}(0292 - 0.0967\omega) \qquad (33)$$

$$V_r^o = 0.33593 - 0.33953 T_r + 1.51941 \cdot T_r^2 - 2.02512 \cdot T_r^3 + 1.11422 \cdot T_r^4 \qquad (34)$$

for $(0 \le T_r \le 0.8)$.

$$V_r^o = 1.0 + 1.3(1 - T_r)^{0.5} \lg(1 - T_r) - 0.50879(1 - T_r) - 0.91534(1 - T_r)^2 \qquad (35)$$

for ($0.8 < \mathrm{Tr} < 1$).

$$\Gamma = 0.29607 - 0.09045T_r - 0.04842 \cdot T_r^2 \qquad (36)$$

Table 3 Data employed for the diffusivities of H_2O_2 and O_2

	T_c [K]	T_o [K]	p_c [bar]	ω	$\tilde{v}_{sc}\left(10^{-5}\frac{m^3}{mol}\right)$	V_r^o	Γ	$\tilde{v}\left[\frac{m^2}{mol}\right]$	$D_{A,H_2O}\left(10^{-9}\left[\frac{m^2}{s}\right]\right)$
H_2O_2	730.2	423.35	209.9	0.331	3.018	0.3811	0.2273	10.63	2.88
O_2	154.6	90.2	50.4	0.025	4.309	0.3820	0.2268	16.37	2.8
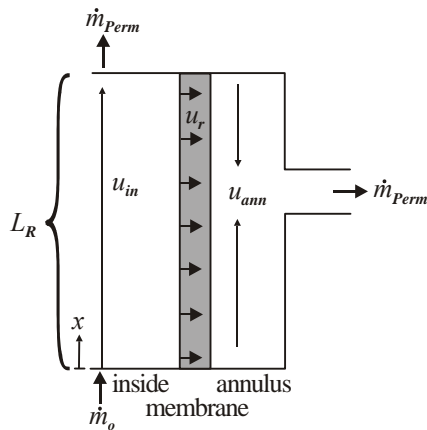
Fig. 6 Fluxes inside the membrane module

Lee-Kessler formula [29]

$$\omega = \frac{\begin{array}{c}-\ln p_c - 5.92714 + 6.09648\theta^{-1} + \\ \hline 15.2518 - 15.6875\theta^{-1} - \end{array}}{\begin{array}{c}+1.28862\ln\theta - 0.169347\theta^6 \\ \hline -13.4721\ln\theta + 0.43577\theta^6\end{array}} \qquad (37)$$

$\theta = T_b/T_c$

The values employed for H_2O_2 and O_2 are given in Table 3.

The axial velocities in the membrane region, the radial velocities in the inner region, and the annulus are neglected. The fluxes are calculated as follows (see Fig. 6). The permeate mass flow $\dot{m}_{perm}$ may be expressed by means of the ratio

$$\chi = \dot{m}_{perm}(t)/\dot{m}_o(t) \qquad (39)$$

Therefore, the total permeate flux, which passes through the membrane from the inlet up to the length x, is given by:

$$\dot{m}_{px}(x,t) = \dot{m}_{perm}(t)x/L_R = \dot{m}_o(t)\chi x/L_R \qquad (40)$$

For the mass flux inside the tube one obtains:

$$\dot{m}_{in}(x,t) = \dot{m}_o(t)(1 - \chi x/L_R) \qquad (41)$$

Assumed that the fluid has a constant density, and the tubular cross section is constant along the tube, the fluid velocity inside the tube is given by:

$$u_{in}(x,t) = u_o(t)(1 - \chi x/L_R) \qquad (42)$$

for ($0.2 \leq T_r \leq 1.0$).

In the annulus is a permeate outlet at the position $x = x_{out}$. Therefore, we find for the mass fluxes in the annulus:

$$\dot{m}_{ann}(x,t) = \begin{cases} \dot{m}_{perm}(t)x/L_R & x < x_{out} \\ 0 & x = x_{out} \\ \dot{m}_{perm}(t)x/L_R - \dot{m}_{perm}(t) & x > x_{out} \end{cases} \qquad (43)$$

The fluid velocities in the annulus are given by:

$$u_{ann}(x,t) = \begin{cases} u_o(t)\theta\chi x/L_R & x < x_{out} \\ 0 & x = x_{out} \\ u_o(t)\theta\chi \cdot (x/L_R - 1) & x > x_{out} \end{cases} \qquad (44)$$

$$\theta = \frac{\text{inner membrane surface}}{\text{outer membrane surface}} \qquad (45)$$

For the partial derivatives one obtains:

$$\frac{\partial u_{in}(t)}{\partial x} = -u_o(t)\chi/L_R \qquad (46)$$

$$\frac{\partial u_{ann}(t)}{\partial x} = -u_o(t)\theta\chi/L_R \qquad (47)$$

For the velocity of the radial flow inside the membrane one obtains:

$$u_r(d,t) = \chi \cdot u_o(t) \cdot d_i^2/(4dL_R) \qquad (48)$$

The inlet velocity of the fluid is given by:

$$u_o(t) = V(t)/A \qquad (49)$$

For the axial dispersion coefficient was calculated according to Taylor and Aris [30,31]:

$$D_{disp} = D_m + \frac{\bar{u}^2 d^2}{192D_m} \qquad (50)$$

For the inner tube and the annulus the values of $D_{disp} = 4.835 \cdot 10^{-3}$ [m²/s] and $D_{disp} = 2.15 \cdot 10^{-4}$ [m²/s] were used, respectively.

The mass transfer coefficient, β, was calculated according to:

$$\beta = Sh \cdot D/d \qquad (51)$$

whereby the Sherwood number is given for the laminar region $\mathrm{Re} < 5 \cdot 10^5$ by:

$$Sh = 0.332 S_c^{1/3}(\mathrm{Re})^{1/2} \qquad (52)$$

and the turbulent region by

$$Sh = 0.0296 \cdot \mathrm{Re}^{0.8} Sc^{0.43} \qquad (53)$$

with the Schmidt number

$$Sc = \eta/(\rho D) \qquad (54)$$

and the Reynolds number

$$Re = (u d \rho)/\eta \qquad (55)$$

The input data given in Table 4 were used for all calculations. A porosity of 0.2779 was used for the Al_2O_3 membrane, and of 0.1405 for the carbon membrane.

Table 4 Input data for the calculation

Reactor length [m]	0.246
Inner diameter of the membrane [m]	0.006
Outer diameter of the membrane [m]	0.010
Position of permeate outlet [m]	0.206
Ratio of permeate flow to inlet flow [-]	1
Density of the fluid [kg/m^3]	1000
Dynamic viscosity of the fluid [Pas]	0.001002
Diffusion resistance factor of the solid membrane [-]	11
Diffusion coefficient in water [m^2/s] H_2O O_2	$2.88 \cdot 10^{-9}$ $2.80 \cdot 10^{-9}$
Inlet concentration [mol/l] H_2O O_2	0.15588 0.0
Ratio of the inner cross section to the annulus cross section [-]	0.81818
Diameter of the outer tube [m]	0.012

Results and discussion

Conversions, fluxes and pressures were measured for the various membranes. An example of the results for the alumina membrane (see no. 1 in Table 1; with 0.3 wt-% Pd, immobilization of Pd with NaOH and reduction with H_2) are given in Fig. 7a/b. After 400 minutes the conversion is constant 98%, the pressure 0.9 bar and the flux 16 l/h. For pore diameter of 0.2 µm (no. 2 in Table 1) the conversion dropped
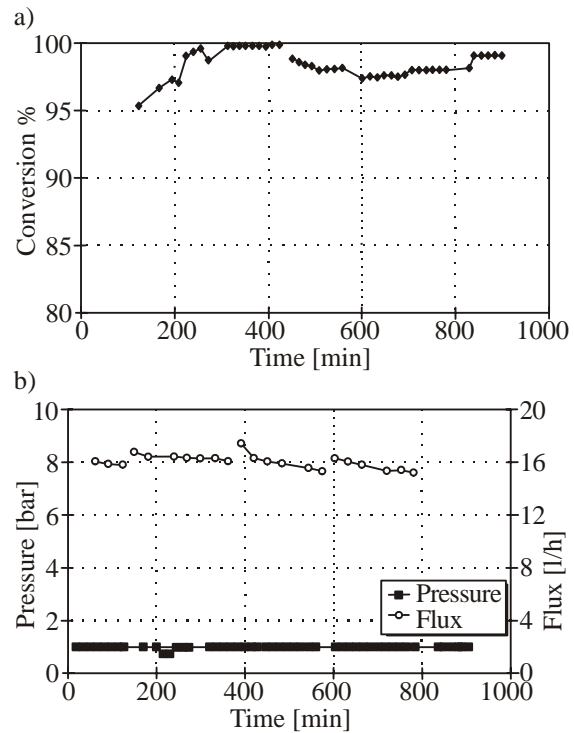
Fig. 7 a) Conversion and b) pressure as a function of time (alumina membrane)
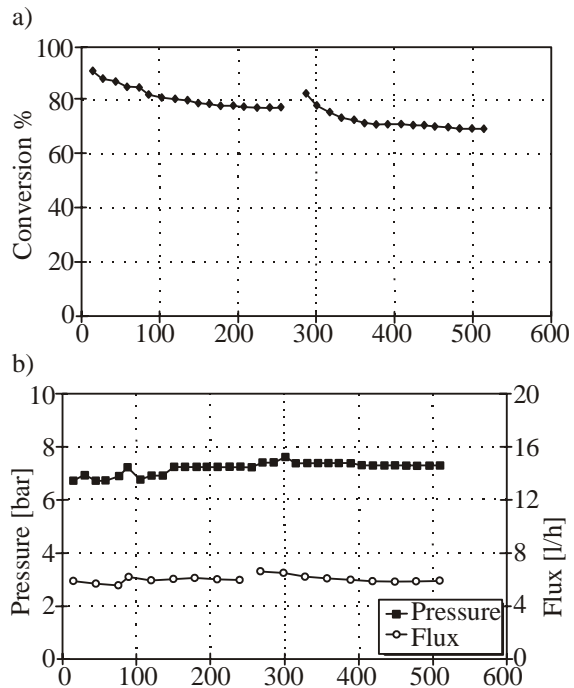
Fig. 8 a) Conversion and b) pressure as a function of time (carbon membrane)

after 900 minutes from 100% to 34% and the flux dropped owing to pore clogging. A reduction of membrane no. 1 in Table 1 with $NaBH_4$ instead of H_2 (0.3 wt-% Pd, immobilization with NaOH) gave a constant conversion of 65%, no pore clogging was observed. If the palladium content of this membrane was reduced from 0.3 wt-% to 0.06 wt-% the conversion was constantly 58% after 1500 min. If the

immobilization of palladium was done with soda the conversion dropped continuiously down to 27%.

The carbon membrane (no. 3 in Table 1, 0.3 wt-% Pd, immobilization with NaOH, reduction with NaBH$_4$) showed a constant conversion of 70% at a flux of 5.5 l/h and a pressure of 7 bar (see Fig 8a/b). A reduction of the palladium content to 0.06 wt-% resulted in a decrease of the conversion to 8% at a flux of 6 l/h. A reduction by means of hydrogen (0.3 wt-% Pd) decreased the conversion from 70% to 42%.

The carbon fiber membranes (no. 4 in Table 1) showed in all cases very low conversions (max. 3%).

The polyethylen membrane (no. 5 in Table 1, 0.3 wt-% Pd, immobilization with NaOH, reduction with NaBH$_4$) gave a constant conversion of 20% at a flux of 14 l/h at a pressure of 4 bar. A reduction of the palladium content to 0.15 wt-% resulted in a decrease of the conversion to 5%. The polypropylen membrane (no. 6 in Table 1; 0.3 wt-% Pd, immobilization with NaOH, reduction with NaBH$_4$) revealed a conversion of only 15% at a flux of 7.5 l/h at a pressure of 4.5bar. Therefore, the polymer membranes gave rather low conversions.

In all cases the 0.2 μm membranes showed a lower conversion compared to the 3 μm membranes, and clogged after a short time. As expected, a higher palladium content led to a higher yield. Furthermore,
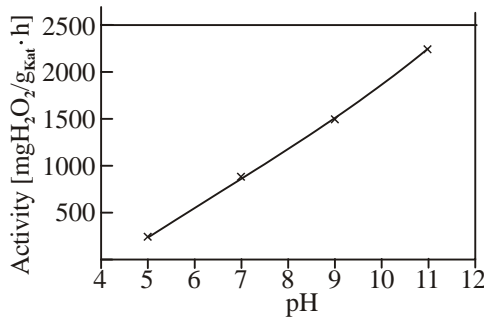
Fig. 9 Activity of the catalyst as a function of the pH value

the membranes with a load of 0.06 wt-% Pd deactivated over the first 200 minutes. The two methods of immobilization of palladium (NaOH, NaCO$_3$) showed no difference in case of the 3 μm alumina membranes, but for 0.2 μm alumina membranes an immobilization by means of NaOH resulted in a higher conversion. The reduction with hydrogen was advantageous for the 3 μm alumina membrane compared to NaBH$_4$; for the 0.2 μm alumina membrane it was just the opposite.

For the other membranes a higher palladium content gave also a higher conversion. The immobilization with NaOH and reduction with NaBH$_4$ led for the carbon membrane to a twice as high conversion as an immobilization at 600°C followed by a reduction with H$_2$. Of considerable importance on the activity of the catalyst is the pH-value. In the range of a pH value of 5 – 11 the activity of the catalyst increased by a factor of about nine (see Fig. 9) for the 3 μm alumina membrane (0.06 wt-% Pd). For all other membranes also a nearly

linear increase of the catalyst activity could be observed with increasing pH value.

The reason for this behaviour may be explained by a mechanism in the alkaline pH region via a perhydroxylion, namely:

$$H_2O_2 + H_2O \Leftrightarrow HO_2^- + H_3O^-$$
$$HO_2^-{}_{(aq)} \Leftrightarrow HO_2^-{}_{(ads)}$$
$$HO_2^-{}_{(ads)} \Leftrightarrow OH^- + O_{(ads)} \qquad (56)$$
$$O_{(ads)} \Leftrightarrow 0.5O_2$$
$$H_3O^+ + OH^- \Leftrightarrow 2H_2O$$
$$\text{-------------------------------------}$$
$$H_2O_2 \Leftrightarrow H_2O + 0.5O_2$$
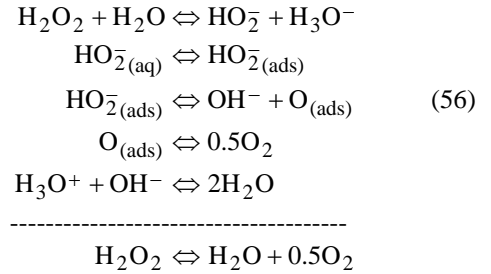
Furthermore, an oxide layer on the catalyst surface may be formed which reacts with perhydroxylions:

$$H_2O_2 \Leftrightarrow H^+HO_2^-$$
$$MO + O_2H^- \Leftrightarrow M + OH^- + O_2 \qquad (57)$$
$$M + O_2H^- \Leftrightarrow MO + OH^-$$
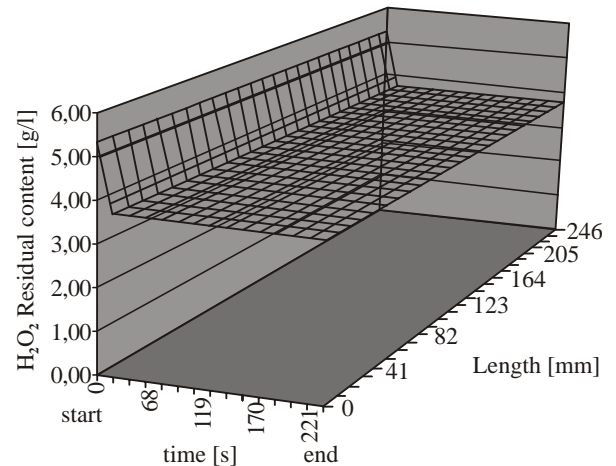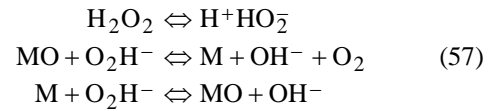
Fig. 10 H$_2$O$_2$ content inside the membrane as a function of time and length
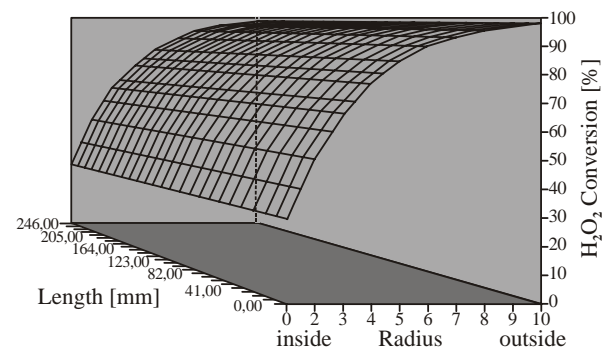
Fig. 11 H$_2$O$_2$ conversion as a function of length and radius

Increasing the temperature leads to an increased decomposition rate, as expected from the kinetic

expression. A variation of the H_2O_2 inlet concentration between 0.25 [g/l] and 70 [g/l] had nearly no influence on the conversion of H_2O_2. This was tested for membrane number one in Table 1, for which the immobilization was done with $NaCO_3$ and reduction with H_2. In the inlet concentration range between 0.25 [g/l] and 40 [g/l] the conversion dropped slightly from 100% to 90%; between 40 [g/l] and 70 [g/l] the conversion increased again to 100%. This may be explained by the change of the reaction order from one to two at higher concentrations. As expected, an increased volume flux, and therefore a shorter contact time, leads to a lower conversion.

Based on the kinetics and the model discussed in the previous sections several simulations were executed. Examples are presented in Figs. 10/11/12. In Fig. 10 the residual content of H_2O_2 as a function of time and length inside the tube is presented for membrane no. 2 in Table 1, where the immobilization was done with NaOH and the reduction with $NaBH_4$. After about 17 [s] a stationary profile is achieved. Stationary profiles of conversion as a function of the membrane radius and length are given in Figs. 11/12. In Fig. 11 the same membrane as in Fig. 10 was calculated. In Fig. 12 a carbon membrane (see no. 3 in Table 1) with a Pd load of 0.06 wt-% was employed.
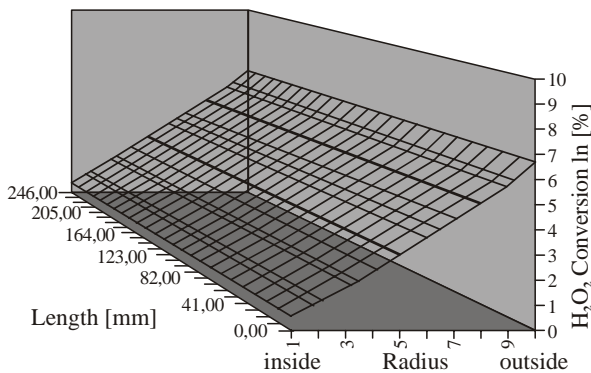
Fig. 12 H_2O_2 conversion as a function of length and radius
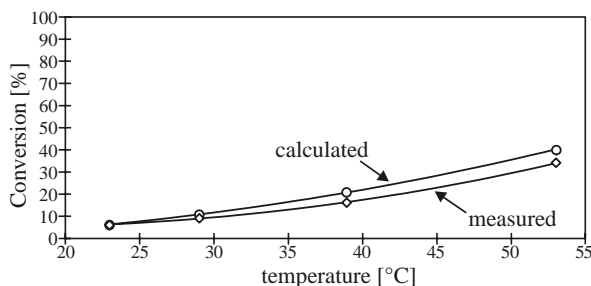
Fig. 13 Comparison of measured and calculated conversions

The immobilization was done by heating to 600°C, and the reduction was executed with H_2. In Figs. 13/14 measured and calculated conversions are compared for various temperatures. As can be seen from the figures, the coincidence is quite good.

In order to test the membranes under real conditions waste water from a plant in Bernburg (Solvay Intox) was investigated. For this purpose the filter was removed from the pilot plant in order to investigate clogging effects. Two alumina membranes were employed (3 µm, 0.2 µm). For both cases a palladium load of 0.3 wt-% was used. The membranes were reduced with $NaBH_4$, the immobilization of palladium was executed by means of NaOH. For the 3 µm membrane a H_2O_2 conversion of 100% could be achieved at a flux of 2.3 l/h at a feed pressure of 1 bar and a flux of 6 l/h at 2 bar. In this case the conversion reduced to 96%. For the 0.2 µm membrane the conversion was 100% at a pressure of 1 bar and a flux of 2.5 l/h. Typical results are presented in Table 5. At a pressure of 1 [bar] nearly all H_2O_2 was decomposed and no pore blocking was observed.

Conclusions

The radial convective flow is a promising alternative for catalytic reactions. Owing to the possibility of varying the pressure one can, at least to a certain extent, control the yield and selectivity of reactions. This approach may be also useful for gas/solid reactions.
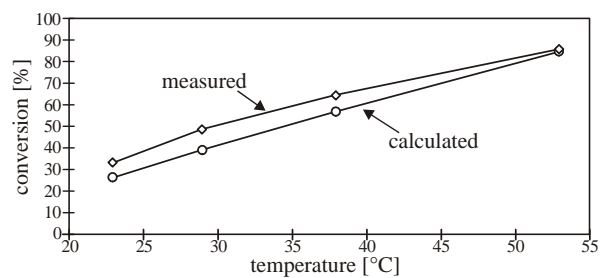
Fig. 14 Comparison of measured and calculated conversions

Table 3 Waste water (Solvay Interox, Bernburg)

	Outlet	After catalytic membrane*
Colour	yellow, opaque	clear
pH	7	7
H_2O_2 [mg/l]	691	0 – 15
COD [mg/l]	943	866
TC [mg/l]	526	494

* 3 µm alumina membranes 0.3 wt-% Pd, immobilization with NaOH, reduction with $NaBH_4$.

SYMBOLS

a	area per unit of length [m]
A	area [m^2]
A_R	cross sectional area [m^2]
c	concentration [mole/m^3]
d	diameter [m]
D	dispersion or diffusion coefficient [m^2/s]
D_m	molecular diffusion coefficient [m^2/s]
i	inner
L_R	length of membrane [m]
$\dot{m}$	mass flow [kg/s]
M	mole weight [g/mole]
n	mole number [mole]
$\dot{n}$	mole flux [mol/s]
$\dot{n}_{ax}$	axial mole flux [mol/s]
n_p	number of components [-]
n_R	number of chemical reactions [-]
p	pressure [Pa]
r	radius [m]
R	rate of reaction [mol/cm^3 ·s]
Re	Reynolds number [-]
$\dot{S}$	total radial flux between phases [mol/s]
Sc	Schmidt number [-]
Sh	Sherwood number [-]
t	time [s]
T	temperature [K]
T_r	reduced temperature [-]
u	flow velocity [m/s]
$\bar{u}$	average flow velocity [m/s]
V	volume [m^3]
V_A	molar volume of diluted A at normal boiling point [cm^3/mole]
x	length coordinate [m]

β	mass transfer coefficient [m/s]
χ	flow ratio [-]
ε	void fraction [-]
Γ	coefficient [-] (see eq. 36)
η	dynamic viscosity [kg/(s · m)]
φ	association factor [-]
v	stoichiometric coefficient [-]
$\tilde{v}$	molar volume
v_j	stoichiometric factor [-]
θ	reduced boiling temperature [-] (see eq. 37), ratio of inner to outer membrane surface [-] (see eq. 45)
ρ	density [kg/m^3]
ω	acentric factor [-]

Subscripts

ann	annulus
ax	axial
c	critical
diff	diffusive
disp	dispersion
in	into
inner	inner side of membrane
membr	membrane
o	inlet
out	out of
outer	outer side of membrane
perm	permeate
r	radial, reduced
rad	radial

REFERENCES

1. Hsieh H.: Catal. Rev.-Sci. Eng. *1991*, 33, 1
2. Hsieh H., in: Membrane Science and Technology Series, Vol. 3, Elsevier, Amsterdam, 1996
3. Zaspalis V.T. and Burggraaf A.J., in: R.R. Bhare (Ed.), Inorganic Membranes. Synthesis, Characteristics and Applications, Van Nostrand Reinhold, New York, 1991
4. Saracco G. and Specchia V.: Catal. Rev.-Sci. Eng. *1994*, 36, 305
5. Zaman J. and Chakma A.: J. Membr. Sci. *1994*, 92, 1
6. Dalmon J.A., in: G. Ertl, H. Knötzinger, J. Weitkamp (Eds.), Handbook of Heterogeneous Catalysis, Vol. 3, Wiley-VCH, Weinheim, 1997.
7. Coronas J. and Santamaria J.: Catal. Today, *1999*, 51, 377
8. Tsotsis T.T., Minet R.G., Champaigne A.M. and Liu P.K.T., in: E.R. Becker and C. Pereira (Eds.), Computer-Aided Design of Catalysts, Marcel Dekker, New York, 1993, p. 471.
9. Marcano J.G.S. and Tsotsis T.T.: Catalytic Membranes and Membrane Reactors, Wiley-VCH, Weinheim, 2002
10. Flügge U.: Entwicklung und Einsatz katalytischer Membranen am Beispiel der Modellreaktion des Wasserstoffperoxidabbaus. Experimentelle und theoretische Untersuchungen. Dissertation, Technische Universität Hamburg-Harburg, 1998
11. Ziegler S., Theis J. and Fritsch D.: J. Membr. Sci. *2001*, 187, 71
12. Vincenta M.J. and Gonzaleza R.D.: AIChE J. *2002*, 48, 1257
13. Kobayashi M., Togawa J., Kanno T., Horinchi J. and Tada K.: J. Chem. Technol. Biotechnol., *2003*, 78, 303
14. Fritsch D., Randjelovic I. and Keil F.: Catal. Today, *2004*, 98, 295
15. Brunelle J.: Pure and Appl. Chem., *1978*, 50, 1211
16. Jiratova K.: Appl. Catal., *1978*, 1, 165.
17. Ludwig S. and Hönicke D.: Chem.-Ing.-Tech., *1992*, 64, 639.
18. McKee D.W.: J. Catal., *1969*, 14, 355
19. Gossner K., Heidrich H. and Körner D.: Z. f. phys. Chem. N.F. *1969*, 67, 220
20. Gossner K. and Bischof H.: Z. f. phys. Chem. N.F. *1972*, 78, 277
21. Gossner K. and Bischof H.: Z. f. phys. Chem. N.F. *1972*, 79, 28
22. Eley D.D. and MacMahon D.M.: J. Coll. Interface Sci., *1972*, 38, 322
23. Kreja L.: Z. f. phys. Chem. N.F., *1984*, 140, 247
24. Schekhobalova V.I.: Vestn. Mosk. Univ., Ser. 2: Khim., *1986*, 27, 97

42

25. Schekhobalova V.I. and Voronova L.V.: Vestn. Mosk. Univ., Ser. 2: Khim., *1989*, 30, 63
26. Numerical Algebra Group Fortran Library, Mark 19, NAG GmbH, Garching
27. Poling B.E., Prausnitz J.M., and O'Connell J.P.: The Properties of Liquids and Gases, McGraw Hill, New York, 2001, Chapter 11.21
28. VDI-Wärmeatlas, VDI-Verlag GmbH, Düsseldorf, 1994
29. Lee B.I., Kessler M.G.: AIChE J., *1975*, 21, 510
30. Taylor, G.: Proc. Royal Soc. A, *1953*, 219, 186
31. Aris R.: Proc. Royal Soc. A, *1956*, 235, 67